Increased Susceptibility to Glaucomatous Damage in Microfibril Deficient Mice

Hang-Jing Wu,[1] John Kuchtey,[1] and Rachel W. Kuchtey[1,2]

[1]Vanderbilt Eye Institute, Vanderbilt University Medical Center, Nashville, Tennessee, United States
[2]Department of Molecular Physiology and Biophysics, Vanderbilt University, Nashville, Tennessee, United States

Correspondence: Rachel W. Kuchtey, Vanderbilt Eye Institute, Vanderbilt University Medical Center, 2311 Pierce Ave, Nashville, TN 37232-8808, USA; rachel.w.kuchtey@vanderbilt.edu.

Received: March 31, 2020
Accepted: July 20, 2020
Published: August 14, 2020

Citation: Wu H-J, Kuchtey J, Kuchtey RW. Increased susceptibility to glaucomatous damage in microfibril deficient mice. *Invest Ophthalmol Vis Sci.* 2020;61(10):28. https://doi.org/10.1167/iovs.61.10.28

Purpose. To test whether mice with microfibril deficiency due to the *Tsk* mutation of fibrillin-1 (*Fbn1*$^{Tsk/+}$) have increased susceptibility to pressure-induced retinal ganglion cell (RGC) degeneration.

Methods. Intraocular pressure (IOP) elevation was induced in *Fbn1*$^{Tsk/+}$ and wild type (wt) mice by injecting microbeads into the anterior chamber. Mice were then followed up for four months, with IOP measurements every three to six days. Retinas were stained for Brn3a to determine RGC number. Optic nerve cross-sections were stained with *p*-phenylene diamine to determine nerve area, axon number, and caliber and thickness of the pia mater.

Results. Microbead injection induced significant IOP elevation that was significantly less for *Fbn1*$^{Tsk/+}$ mice compared with wt. The optic nerves and optic nerve axons were larger, and the elastic fiber-rich pia mater was thinner in *Fbn1*$^{Tsk/+}$ mice. Microbead injection resulted in reduced optic nerve size, thicker pia mater, and a slight decrease in axon size. *Fbn1*$^{Tsk/+}$ mice had significantly greater loss of RGCs and optic nerve axons compared with wt (14.8% vs. 5.8%, $P = 0.002$, and 17.0% vs. 7.5%, $P = 0.002$, respectively).

Conclusions. *Fbn1*$^{Tsk/+}$ mice had altered optic nerve structure as indicated by larger optic nerves, larger optic nerve axons and thinner pia mater, consistent with our previous findings. Despite lower IOP elevation, *Fbn1*$^{Tsk/+}$ mice had greater loss of RGCs and optic nerve axons, suggesting increased susceptibility to IOP-induced optic nerve degeneration in microfibril-deficient mice.

Keywords: glaucoma, microbead injection, fibrillin-1, axon degeneration, elastic fiber

Glaucoma is the leading cause of irreversible blindness and is due to the progressive degeneration of retinal ganglion cells (RGCs) and their axons.[1] Many risk factors, such as age, intraocular pressure (IOP), and race have been identified. Although the precise pathogenesis of glaucoma is still under intense investigation, it has long been recognized that the initial injury site of RGC axonal damage occurs at optic nerve head (ONH).[2] The concept of the ONH as a biomechanical structure,[3] particularly when challenged by elevated IOP, has been described both experimentally[4–6] and through computer modelling.[7–11] Substantial evidence supports the hypothesis that the biomechanical properties of ONH connective tissues and their responses to IOP-related stress are key determinants of susceptibility to glaucomatous optic nerve damage.[3,12] Identification of specific features of ONH connective tissue that render certain populations more susceptible to developing glaucoma will facilitate our understanding of disease pathogenesis.

A key component of the extracellular matrix (ECM), microfibrils are composed of fibrillins and fibrillin-associated glycoproteins, which contribute to mechanical properties of a variety of tissues, such as ocular, aortic and dermal connective tissue.[13] Fibrillin-1, encoded by the *FBN1* gene, is the major structural component of microfibrils. Although microfibrils can form fibrous structures on their own, most commonly they ensheathe the elastin core of elastic fibers. The elastic fiber-rich pia mater is the innermost layer of the optic nerve meninges, which is tightly wrapped around the optic nerve and is thought to be crucial for load-bearing.[14,15] Previously, we found that the pia mater of *Fbn1*$^{Tsk/+}$ is thinner than wt, suggesting altered biomechanical properties of the optic nerve.[16] Likewise, the ECM in the aorta has been shown to play a fundamental role in sensing and responding to mechanical stress.[17,18] In a mouse model of Marfan syndrome (MFS), which is caused by microfibril defects due to a mutation in *Fbn1* (*Fbn1*$^{C1039/+}$), elastic fiber lamelli in the aorta are disrupted, contributing to aneurism formation and eventual dissection.[19,20] A weakened pia mater could result in an optic nerve more sensitive to mechanical stress, rendering the optic nerve more vulnerable to pressure-induced damage. The prevalence of glaucoma in MFS is higher than in the general population, supporting the idea that microfibril defects contribute to glaucoma.[21] In addition, racial differences in the expression of ECM components including fibrillin in the optic nerve could partially explain the varying prevalence of glaucoma in different populations.[22] Alterations in the elastic fiber structure have been implicated in the pathology of glaucoma, specifically in pseudo-exfoliation glaucoma.[23,24] Downregulation of elastic fiber components such as

fibrillin-1 and elastin in the lamina cribrosa has been reported in exfoliation syndrome-associated glaucoma.[23,24] These findings support our hypothesis that microfibril abnormalities in optic nerve head tissue play a key role in glaucoma pathogenesis.

Identification of the microfibril-associated *ADAMTS* gene family in dog models of primary open angle glaucoma[25–28] and human glaucoma patients[29–31] support the hypothesis that microfibril defects cause glaucoma.[32] To test this hypothesis in a previous study, we characterized glaucomatous phenotypes in a mouse line with known microfibril deficiency due to heterozygosity of the *Tsk* mutation of *Fbn1* (*Fbn1*$^{Tsk/+}$). The *Tsk* mutation is an in-frame duplication of exons 17 to 40 in *Fbn1* that results in a larger-than-normal protein. The mutant protein can copolymerize with normal fibrilin-1 but results in functionally deficient microfibrils.[33] We found that although *Fbn1*$^{Tsk/+}$ mice did not display accelerated loss of RGC axons, they do have several ocular phenotypes that may be relevant to glaucoma pathogenesis, particularly expansion of the optic nerve and optic nerve axons, which occur in the setting of normal IOP.[16] In the DBA/2J mouse model of glaucoma, which display spontaneous IOP elevation at advanced age, axons expand before frank loss, suggesting that axonal enlargement predicts degeneration.[34] Moreover, age-related axon expansion was reported in C57BL/6J mice.[35,36] With their optic nerve and optic nerve axon expansion and thinner pia mater, we hypothesized that *Fbn1*$^{Tsk/+}$ mice would be more susceptible to elevated IOP as an additional stressor.

The objective of this study was to test the hypothesis that microfibril-deficient mice are susceptible to pressure-induced RGC damage. To this end, microbeads were injected unilaterally for inducing IOP elevation, IOP was monitored, and RGC degeneration was characterized. Although microfibril deficient mice have lower IOP responses, greater magnitudes of RGC axon and cell loss were detected compared with the wt mice, supporting our hypothesis.

Methods

Animals and Tissue Collection

This study was performed in accordance with the Association for Research in Vision and Ophthalmology Statement for the Use of Animals in Ophthalmic and Vision Research and with approval by the Institutional Animal Care and Use Committee of Vanderbilt University. Male *Fbn1*$^{Tsk/+}$ and female wt mice, both on the C57BL/6J background, were obtained from The Jackson Laboratory and bred in house to produce wt and *Fbn1*$^{Tsk/+}$ experimental animals. Mice were housed in a facility operated by the Vanderbilt University Division of Animal Care with a 12-hour light/dark cycle with standard chow and water provided as desired.

Male and female mice seven months of age at the time of microbead or sham injections (see below) were used for experiments. This age was chosen because we previously found expanded optic nerves starting at six months of age[16] and to avoid a potential protective effect of advanced age that has been reported for 10- to 12-month-old C57BL/6J mice.[37,38] Four months after injection, mice were euthanized by carbon dioxide inhalation followed by thoracotomy and then cardiac perfused with 10 mL phosphate-buffered saline solution (PBS) followed by 10 mL 4% paraformaldehyde (PFA)/PBS. Eyes were enucleated, and the optic nerves cut ~1.5 mm from the globe and at the optic chiasm and then placed in 1% glutaraldehyde/4% PFA in PBS. A total of 98 mice were used for this study, including 45 wt and 31 *Fbn1*$^{Tsk/+}$ mice that received microbead injections and 12 wt and 10 *Fbn1*$^{Tsk/+}$ mice that received sham injections. All mice were included in the data analysis except those for which tissue harvesting or processing was unsuccessful.

Microbead Injection

After dilation of the right eye by application of 1% atropine (Akorn, Lake Forest, IL, USA), mice were anesthetized with 2.5% isoflurane in oxygen delivered by a precision vaporizer (Vet Equip, Livermore, CA, USA). For bead-injected mice, the anterior chamber of the right eye was injected with 2 µL of 6 µm diameter polystyrene beads (Cat. no. 18136, Polysciences, Inc., Warrington, PA, USA), followed by 1 µL of sodium hyaluronate viscoelastic material (Healon OVD 10 mg/mL; Johnson & Johnson Vision, Santa Ana, CA, USA).[38] Microbeads were sterilized before injection following a previously published protocol by treatment with 100% ethanol[38] for 10 minutes. After washing in PBS, the beads were pelleted and then loaded into a glass micropipette.[36,37] For microbead delivery, corneas were gently punctured with the micropipette that had been filled first with viscoelastic followed by microbeads. After delivery of beads and viscoelastic, the micropipette was held in place for two minutes and then slowly withdrawn to avoid reflux. To precisely control the volume of microbeads delivered, a pipettor was used to measure 2-µL volumes of microbeads to be loaded into the glass micropipette. For sham controls, the right eye was injected as above, except PBS was substituted for microbeads. Left eyes were not injected to serve as contralateral intra-animal controls. Mice with damage to the iris or lens during injection were removed from the study.

IOP Measurement

IOP of both eyes (right eye first) of isoflurane-anesthetized mice was measured using a rebound tonometer (TonoLab, iCare, Helsinki, Finland), with measurements completed within two minutes of loss of consciousness to avoid anesthetic effects[39] and at the same time of day to avoid diurnal fluctuations[40] and calculated as the average of three separate determinations. IOP was measured every three days during the first month, then every six days during the following three months after injection. ΔIOP for each animal was calculated as IOP of the injected eye minus the contralateral eye at each time point. Positive integrated ΔIOP for each animal was calculated as the area under the ΔIOP versus time curve, with negative values set to zero.

Immunostaining of Retinal Whole Mounts and RGC Quantification

Retinas were dissected from enucleated eyes and stained for the RGC-specific marker Brn3a[41] as described previously.[16] Briefly, retinas were stained 40 hours at 4°C with goat polyclonal anti-Brn3a antibody (cat. no. sc-31984; Santa Cruz Biotechnology, Dallas, TX, USA), diluted in blocking buffer (5% normal donkey serum in 0.5% Triton X-100 in PBS), then washed and incubated for three hours at room temperature in donkey anti-goat immunoglobulin G Alexa Fluor 488 (Thermo Fisher Scientific, Waltham, MA, USA). Montage images (×20) of the entire retina were assembled using

Investigative Ophthalmology & Visual Science

Nikon NIS-Elements software from image tiles acquired with a Nikon Eclipse Ti microscope (Nikon, Tokyo, Japan). RGCs were counted from the entire retina using a semi-automated method described by Geeraerts et al.[42]

Optic Nerve Staining, Axon Quantitation and Pia Mater Thickness Determination

Optic nerves were fixed in 2% osmium in PBS for one hour, dehydrated, and embedded in epon as described previously.[16] Thin cross-sections (1 μm) of optic nerves were cut at approximately 1.5 mm from the globe using an EM UC7 ultramicrotome (Leica, Wetzlar, Germany). Sections were stained with *p*-phenylene diamine (PPD), then mounted using Permount Mounting Medium (Thermo Fisher Scientific).

Nerve images were acquired using an inverted microscope equipped with a 100× 1.45 NA oil immersion objective and DS-Ri2 camera (Nikon). Montage Images of the entire nerve were assembled in NIS-Elements software (Nikon) and analyzed in Fiji (https://imagej.net/Fiji). Nerve area (not including the pia mater) was determined as the area of a polygon drawn around the nerve. The total number and size of axons were determined using AxonJ, an automated counting plugin for Fiji developed by Zarei et al.[43] AxonJ counting accuracy was validated by comparing to manual counts of optic nerves from another data set, in which the total axon number was calculated by multiplying the manually determined axon density (determined by counting axons within 24 boxes covering ~10% of the optic nerve area) by the nerve area. AxonJ, gave counts that were ranged from 83% to 120% of manual counts. AxonJ size accuracy was determined by comparison to another data set in which axon area of >10,000 axons in 19 nerves was determined manually. AxonJ gave mean axon areas that ranged from 92% to 137% of the manual determinations.

Pia mater thickness was determined in the same PPD-stained nerve cross-sections used for determining axon counts. The area of the nerve including the pia mater (A_{total}) and the area of the nerve not including the pia mater (A_{inner}) were determined using the polygon drawing function of NIH ImageJ (Supplementary Fig. S1). The area of the pia mater was determined as $A_{total} - A_{inner}$. To determine the pia mater thickness, the outer radius of the nerve including the pia mater (R_o) was calculated as equal to the square root of A_{total}/π and the inner radius not including the pia mater (R_i) was calculated as the square root of A_{inner}/π. Pia mater thickness was then calculated as $R_o - R_i$.

Histologic Staining

Optic nerve glial lamina sections 7 µm thick were deparaffinized and hydrated. Sections were oxidized in 10% oxone (Sigma, St. Louis, MO, USA) for 40 minutes, washed, then incubated in Weigert' s Resorcin Fuchsin solution (Electron Microscopy Sciences, Hatfield, PA, USA) for one hour. After clearing in 95% ethanol, sections were stained in Weigert's iron hematoxylin solution (Electron Microscopy Sciences) for 10 minutes, then counterstained with van Gieson's solution (Electron Microscopy Sciences) for 30 seconds. Slides were rinsed in distilled water, dehydrated in 95% ethanol, cleared in xylene, and then mounted.

Statistical Analysis

Statistical analysis was performed using GraphPad Prism or Python (https://www.python.org). Comparisons between two groups were performed using Student's *t*-tests or Mann-Whitney tests. Percentage RGC loss or axon loss relative to the population mean was calculated as follows: for each mouse, the difference between the number in the injected eye and the average number of the uninjected eyes of the same genotype was divided by the average number of the uninjected eyes of the same genotype. Data are presented as mean ± standard error of the mean (SEM). Numbers of samples are stated in the figure legends. Approximately equal numbers of male and female animals were included in experiments.

Results

Lower IOP Response to Microbead Injection in *Fbn1*$^{Tsk/+}$ Mice

Previously, we showed that *Fbn1*$^{Tsk/+}$ mice have expanded optic nerves with enlarged optic nerve axons, which we hypothesized could result in increased susceptibility to IOP-induced RGC degeneration.[16] To test this hypothesis, the anterior chambers of the right eyes of seven-month-old wt and *Fbn1*$^{Tsk/+}$ mice were injected with polystyrene beads followed by 1 µL of sodium hyaluronate to induce elevation of IOP, with the left eyes not injected to serve as contralateral controls. As shown in Figures 1A and 1B, microbead injection induced significant elevation of IOP compared with uninjected control eyes of both wt and *Fbn1*$^{Tsk/+}$mice that was sustained over the four-month postinjection period. An unanticipated result, apparent in Figures 1A and 1B, is that IOP elevation was much less for *Fbn1*$^{Tsk/+}$ mice compared with wt. Bead-induced ΔIOP (injected minus uninjected eye) was significantly greater for wt compared with *Fbn1*$^{Tsk/+}$ mice (Fig. 1C), with average ΔIOP over the four-month period of 5.8 ± 1.1 mm Hg for wt but only 2.8 ± 1.0 mm Hg (mean ± SEM) for *Fbn1*$^{Tsk/+}$ mice. Quantifying IOP responses by integrating ΔIOP over time (Fig. 1D) shows lower magnitude responses of *Fbn1*$^{Tsk/+}$ mice compared with wt (mean ± SEM: 398 ± 43 for *Fbn1*$^{Tsk/+}$ vs. 708 ± 78 mm Hg days for wt, $P = 0.0016$, analysis of variance (ANOVA) with Sidak's multiple comparisons test). A small elevation of IOP was observed in sham control eyes that were injected with PBS instead of microbeads (mean ± SEM: 158 ± 13 for wt and 204 ± 12 mm Hg days for *Fbn1*$^{Tsk/+}$ mice), with no significant difference between *Fbn1*$^{Tsk/+}$ and wt ($P = 0.95$, Fig. 1D).

Optic Nerve Size

Consistent with our previous finding of enlarged optic nerves in *Fbn1*$^{Tsk/+}$ mice,[16] optic nerves from uninjected eyes were significantly larger for *Fbn1*$^{Tsk/+}$ mice as compared with wt (Fig. 2A). Combining data from uninjected eyes from sham and microbead injection groups, the optic nerve area of *Fbn1*$^{Tsk/+}$ mice was 7.6% larger than wt (0.101 ± 0.002 mm^2 for *Fbn1*$^{Tsk/+}$ vs. 0.094 ± 0.001 mm^2 for wt, $P = 0.0001$, Student's *t*-test). This confirmation of increased nerve size indicates abnormal optic nerve structure in *Fbn1*$^{Tsk/+}$ mice.

Microbead injection induced a significant size reduction of the optic nerves (Fig. 2B) of both wt and *Fbn1*$^{Tsk/+}$ mice ($P = 0.004$ and 0.0006, respectively, Student's *t*-test). Compared

Investigative Ophthalmology & Visual Science

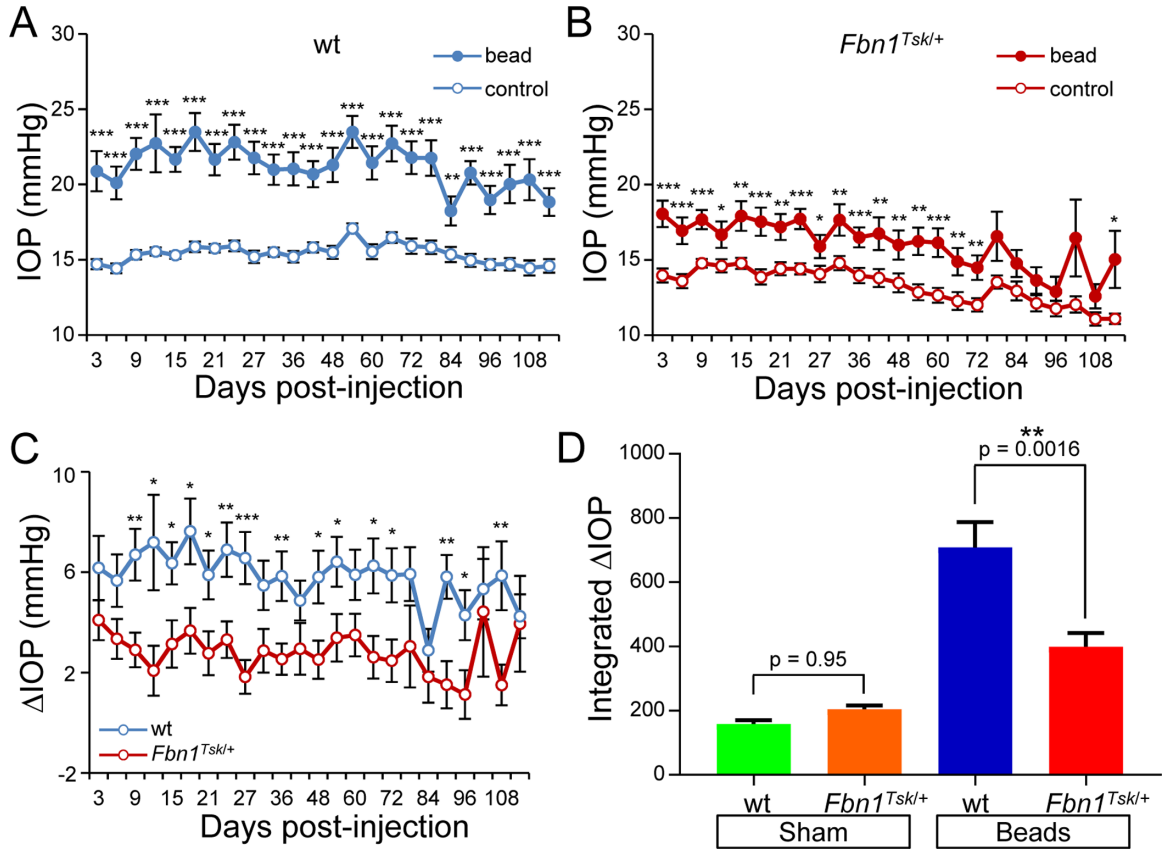

Figure 1. IOP responses to microbead injections. Microbead-injected eyes (*filled symbols*) developed sustained elevations of IOP above that of uninjected control eyes (*open symbols*) for wt (**A**), with lower magnitude responses for *Fbn1*$^{Tsk/+}$ mice (**B**). ΔIOP (injected minus uninjected IOP) was significantly lower for *Fbn1*$^{Tsk/+}$ mice (*red symbols*) compared to wt (*blue symbols*, **C**). Integrated ΔIOP was significantly lower in magnitude for *Fbn1*$^{Tsk/+}$ mice (red bar) compared to wt (*blue bar*), whereas sham injections induced a small elevation of integrated ΔIOP that was not different between wt (*green bar*) and *Fbn1*$^{Tsk/+}$ mice (*orange bar*, **D**). Numbers of microbead-injected animals: 45 wt and 31 *Fbn1*$^{Tsk/+}$; sham-injected: 12 wt and 10 *Fbn1*$^{Tsk/+}$. Statistical significance assessed by Student *t*-tests (paired for **A** and **B**, unpaired for **C**) or ANOVA followed by Sidak's multiple comparisons tests (**D**) are indicated: $^{*}P < 0.05$; $^{**}P < 0.01$; $^{***}P < 0.001$.

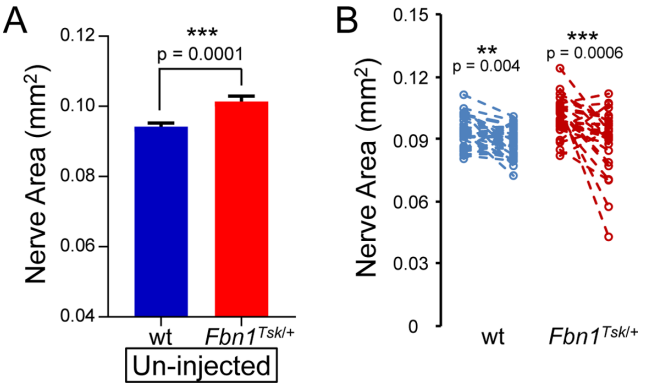

Figure 2. Reduced nerve size in response to microbead injection. Comparing un-injected eyes, *Fbn1*$^{Tsk/+}$ mice had enlarged optic nerves compared to wt (A). Analysis (B) comparing uninjected (*left symbols*) with bead-injected eyes (*right symbols*) showed significant reduction in cross-sectional area of nerves from wt (*blue symbols*) and *Fbn1*$^{Tsk/+}$ mice (*red symbols*) but not for sham-injected controls (data not shown). Numbers of microbead-injected animals: 43 wt and 29 *Fbn1*$^{Tsk/+}$: sham-injected: 12 wt and 9 *Fbn1*$^{Tsk/+}$. *Dashed lines* connect paired eyes (**B**).

to un-injected controls, cross-sectional area of nerves from bead-injected eyes was reduced by 4.2 ± 1.3% in wt and 11.1 ± 2.9% in *Fbn1*$^{Tsk/+}$ mice (mean ± SEM). The percent decrease in nerve area induced by bead injection was greater for *Fbn1*$^{Tsk/+}$ mice than it was for wt (p = 0.04). Sham injections did not induce significant reductions in nerve area for wt ($P = 0.42$) and *Fbn1*$^{Tsk/+}$ ($P = 0.85$, Student's *t*-test).

Pia Mater Thickness

In cross-sections of the optic nerve at the glial lamina region, Weigert's resorcin fuchsin counterstained with van Gieson's staining revealed a network of elastic fibers within a collagen matrix that occupies the full thickness of the pia mater that stained purple (Fig. 3A). Comparing uninjected eyes (Fig. 3B), the pia mater was 28.7% thinner in optic nerves from *Fbn1*$^{Tsk/+}$ mice (2.5 ± 0.09 μm, mean ± SEM) compared with those from wt (3.8 ± 0.10 μm, $P < 0.0001$, Student's *t*-test), consistent with our previous finding.[16] In addition, the area of the pia mater was 31% smaller in nerves from uninjected eyes of *Fbn1*$^{Tsk/+}$ mice compared those from wt (0.0029 ± 0.0001 vs. 0.0042 ± 0.0001 mm^2, mean ± SEM, $P = 3.1 \times 12^{-12}$, Student's *t*-test), indicating that thinning was not simply due to increased inner radius of the optic nerve but represents reduction of pia mater tissue. The abnormal

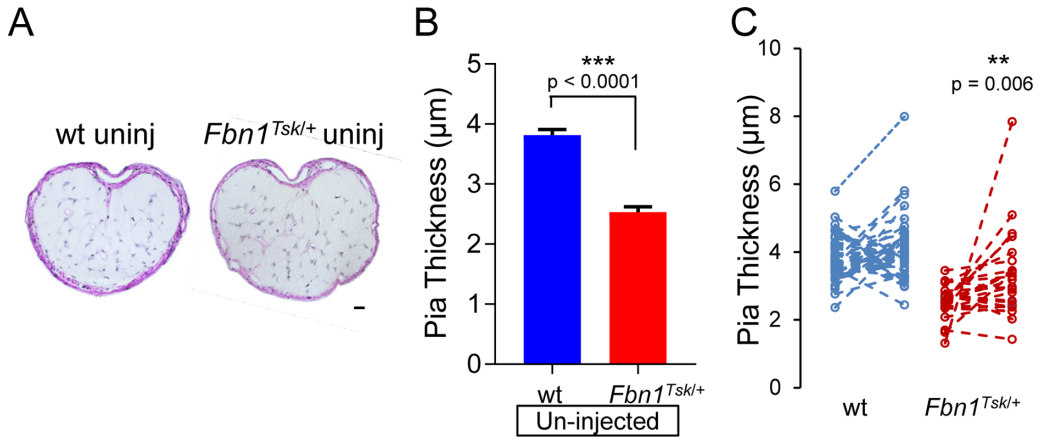

Figure 3. Thickening of the pia mater in optic nerves from bead-injected eyes. Representative images of optic nerve cross-sections of uninjected eyes of wt and *Fbn1*$^{Tsk/+}$ mice stained with Weigert's resorcin fuchsin and hematoxylin showing the pia mater stained purple (**A**). Comparing uninjected eyes, *Fbn1*$^{Tsk/+}$ mice had thinner pia mater as compared to wt (**B**). Analysis (**C**) comparing nerves from uninjected (*left symbols*) with those from bead-injected eyes (*right symbols*) showed significant increase in pia mater thickness in response to bead injection for *Fbn1*$^{Tsk/+}$ mice (*red symbols*), but not for wt (*blue symbols*). Numbers of animals: 37 wt and 25 *Fbn1*$^{Tsk/+}$. *Scale bar* in A: 20 µm. *Dashed lines* connect paired eyes (C).

pia mater suggests significant alterations in the extracellular matrix of the optic nerve in *Fbn1*$^{Tsk/+}$ mice that would likely impact biomechanical properties of the tissue and responses to elevated IOP.

Analysis comparing bead-injected and contralateral controls (Fig. 3C) showed that microbead injection resulted in thickening of the pia mater that reached statistical significance for *Fbn1*$^{Tsk/+}$ mice ($P = 0.006$, Student's *t*-test, Fig. 3C) but not for wt. Bead injection also caused an increase in the area of the pia mater that was statistically significant for *Fbn1*$^{Tsk/+}$ mice ($P = 0.035$, Student's *t*-test) but not for wt, suggesting that an increase in the amount of pia mater tissue contributed to its thickening. Thickening of the pia mater in nerves from bead-injected eyes suggests connective tissue remodeling of the optic nerve in response to elevated IOP.

RGCs

To determine RGC loss induced by microbead injection, immunofluorescent staining for the RGC-specific marker Brn3a was performed on whole-mount retinas. Heat maps of RGC density (Fig. 4A) showed lower density in the superior and nasal quadrants for all retinas, similar to our previous findings with manual RGC counting.[16] The extent of RGC loss in microbead-injected eyes varied between individual mice, ranging from mild to severe damage (Fig. 4A).

Analysis of bead-injected and contralateral control eyes (Fig. 4B) showed significant loss of RGCs in bead-injected eyes for both wt ($P = 0.003$) and *Fbn1*$^{Tsk/+}$ mice ($P = 0.0004$) but not for sham-injected mice ($P > 0.39$, Student's *t*-test). Microbead injection and genotype significantly contributed to percentage RGC loss (Fig. 4C, $P < 0.0001$ and $P = 0.02$, respectively) with significantly greater loss in the microbead-injected eyes of *Fbn1*$^{Tsk/+}$ mice as compared to wt (mean ± SEM: 14.8 ± 3.6% for *Fbn1*$^{Tsk/+}$ and 5.8 ±1.7% for wt, $P = 0.002$, two-way ANOVA with Sidak's multiple comparisons test). In the sham group, there was no significant difference in percentage RGC loss in either wt or *Fbn1*$^{Tsk/+}$ mice (not shown, two-way ANOVA).

Optic Nerve Axons

To determine the effect of microbead injection on RGC axons, postlaminar optic nerve cross-sections were stained with PPD and imaged by high-resolution light microscopy. The extent of axon loss in bead-injected eyes varied considerably between mice, with some nerves displaying obvious focal regions of severe damage (Fig. 5A, red asterisks). Focal axon loss in response to microbead injection was significantly more common in *Fbn1*$^{Tsk/+}$ mice, displayed by six of 29 nerves (20.6%), compared with one of 43 nerves (2.3%) for wt ($P = 0.01$, Fisher's exact test). Sham injected nerves appeared normal (not shown).

Significant loss of axons in bead-injected compared to contralateral control eyes was found for both wt ($P = 1.8 \times 10^{-4}$) and *Fbn1*$^{Tsk/+}$ mice ($P = 3.7 \times 10^{-4}$), but not for sham-injected mice ($P > 0.72$, Fig. 5B, Student's *t*-test). Microbead injection and genotype significantly contributed to percentage axon loss (Fig. 4C, $P < 0.0001$ and $P = 0.03$, respectively) with significantly greater loss in nerves from microbead-injected eyes of *Fbn1*$^{Tsk/+}$ mice as compared with wt (mean ± SEM: 17.0% ± 4.0% for *Fbn1*$^{Tsk/+}$ and 7.5% ±1.5% for wt, $P = 0.004$, two-way ANOVA with Sidak's multiple comparisons test). In the sham group, there was no significant difference in percentage axon loss in either wt or *Fbn1*$^{Tsk/+}$ mice (not shown, two-way ANOVA). These results show that despite having lower IOP responses to bead injection, *Fbn1*$^{Tsk/+}$ mice experienced greater axon loss, indicating greater susceptibility to IOP-induced degeneration.

Axon Size

Previously by manual determination of axon size, we had shown that *Fbn1*$^{Tsk/+}$ mice have enlarged axons at six and 16 months of age and found that axon enlargement progresses with age.[16] We hypothesized that axon enlargement may result in increased susceptibility to pressure-induced damage. Enlargement of optic nerve axons at 11 months of age was confirmed in the current data set by analysis of axon size of individual nerves using the program AxonJ (Fig. 6A), which showed median axon diameters from

Investigative Ophthalmology & Visual Science

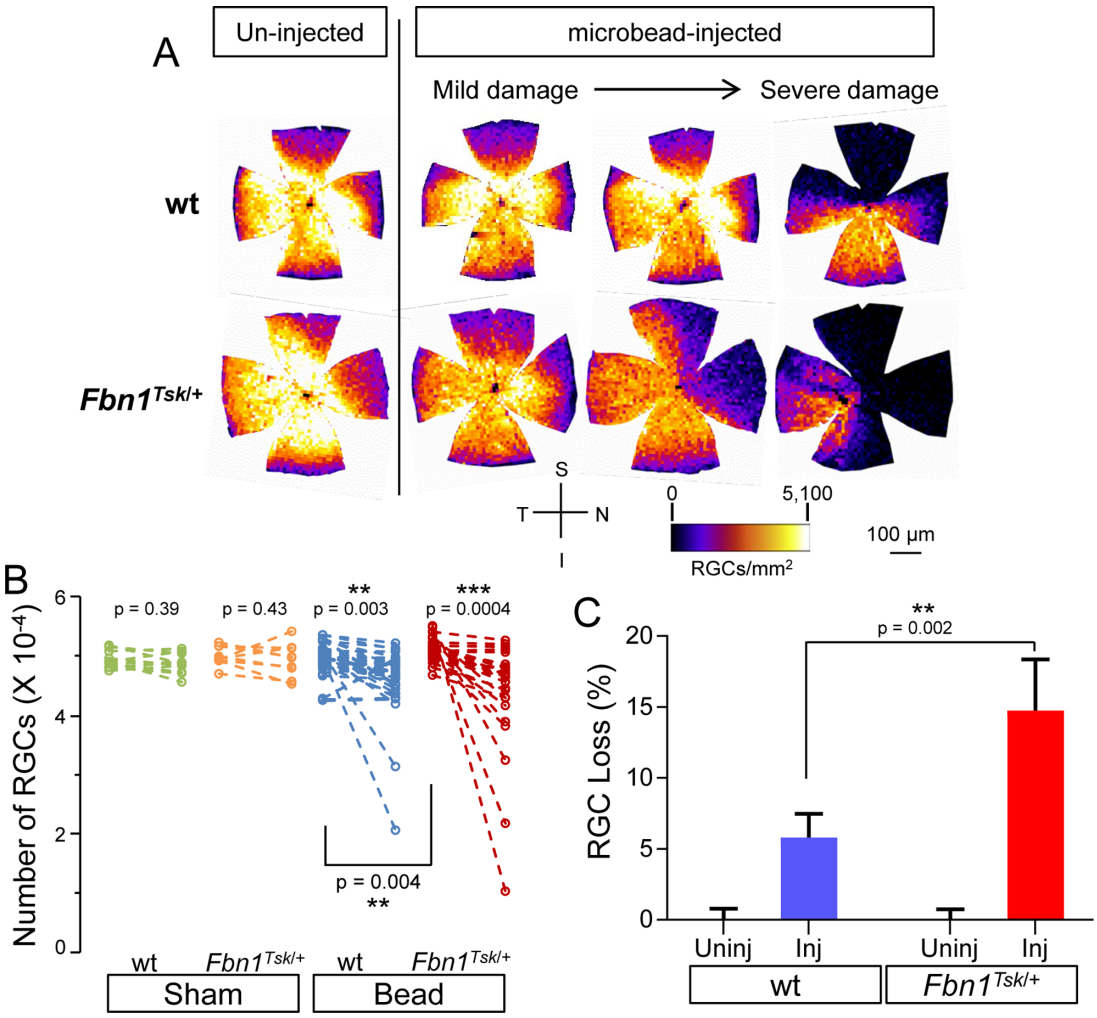

Figure 4. RGC loss in response to microbead injection. Heat maps of RGC density (**A**) show that compared to retinas from un-injected eyes (*left column*), microbead injection resulted in decreased RGC density in wt (*top row*) and *Fbn1*$^{Tsk/+}$ mice (*bottom row*) with variability between individual mice ranging from mild to severe damage, as well as lower densities in the superior and nasal quadrants. Analysis (**B**) comparing uninjected (*left symbols*) with bead-injected eyes (*right symbols*) showed significant loss of RGCs for wt (*blue symbols*) and *Fbn1*$^{Tsk/+}$ mice (*red symbols*) but not for sham-injected controls (*green* and *orange symbols*). The average percent RGC loss relative to the average number of RGCs in uninjected eyes (**C**) was lower for wt (*blue bar*) as compared with *Fbn1*$^{Tsk/+}$ mice (*red bar*). Orientation of retinal whole mounts (S: Superior, N: Nasal, I: Inferior and T: Temporal) and heat map density scale are shown (**A**). Numbers of microbead-injected animals: 43 wt and 26 *Fbn1*$^{Tsk/+}$: sham-injected: 12 wt and 10 *Fbn1*$^{Tsk/+}$. *Dashed lines* connect paired eyes (**B**).

individual mice 2.4% larger in *Fbn1*$^{Tsk/+}$ nerves compared to wt (0.881 ± 0.006 μm for *Fbn1*$^{Tsk/+}$ and 0.860 ± 0.003 μm for wt, mean ± SEM, $P = 0.0005$, Student's *t*-test). In addition, comparison of pooled axon diameters of all nerves from uninjected eyes (1,105,075 wt axons and 1,014,017 *Fbn1*$^{Tsk/+}$ axons, Fig. 6B) shows a rightward shift in the size distribution, with median axon diameter 2.6% larger for *Fbn1*$^{Tsk/+}$ compared with wt mice (median diameters 0.880 μm for *Fbn1*$^{Tsk/+}$ and 0.858 μm for wt, $P < 0.001$, Mann-Whitney U-test), confirming that axons were enlarged in nerves from *Fbn1*$^{Tsk/+}$ mice.

To determine whether axon size was affected by microbead injection, comparisons were made between median axon sizes of individual mice (Fig. 6C) and between the size distributions of axons pooled from each group (Figs. 6D and 6E). Comparing the median axon diameter of bead-injected eyes of individual mice to the average median axon size of uninjected eyes of the same genotype (Fig. 6C) suggested that axon size was not altered by microbead injection ($P > 0.33$, Student's *t*-test). However, analysis of pooled axons (Figs. 6D and 6E) showed that microbead injection resulted in a slight decrease in median axon diameter compared to un-injected nerves that was similar in wt and *Fbn1*$^{Tsk/+}$ mice (0.85% for wt and 0.81% for *Fbn1*$^{Tsk/+}$. For wt, the median diameter was 0.858 μm for uninjected versus 0.851 for bead-injected, and for *Fbn1*$^{Tsk/+}$ mice the median diameters were 0.880 μm for un-injected *vs*. 0.872 for bead-injected, $P < 0.001$, Mann-Whitney U test. Although this would indicate a slightly higher susceptibility of larger than average axons, the shapes of the axon size distributions (Figs. 6D and 6E) were very similar with little or no change in the percentage of large axons having diameters above 1.2 μm in diameter. Analysis of axon size distributions including only mice with > 20% axon loss or including only those with 5% to 20% loss yielded similar results (data not shown).

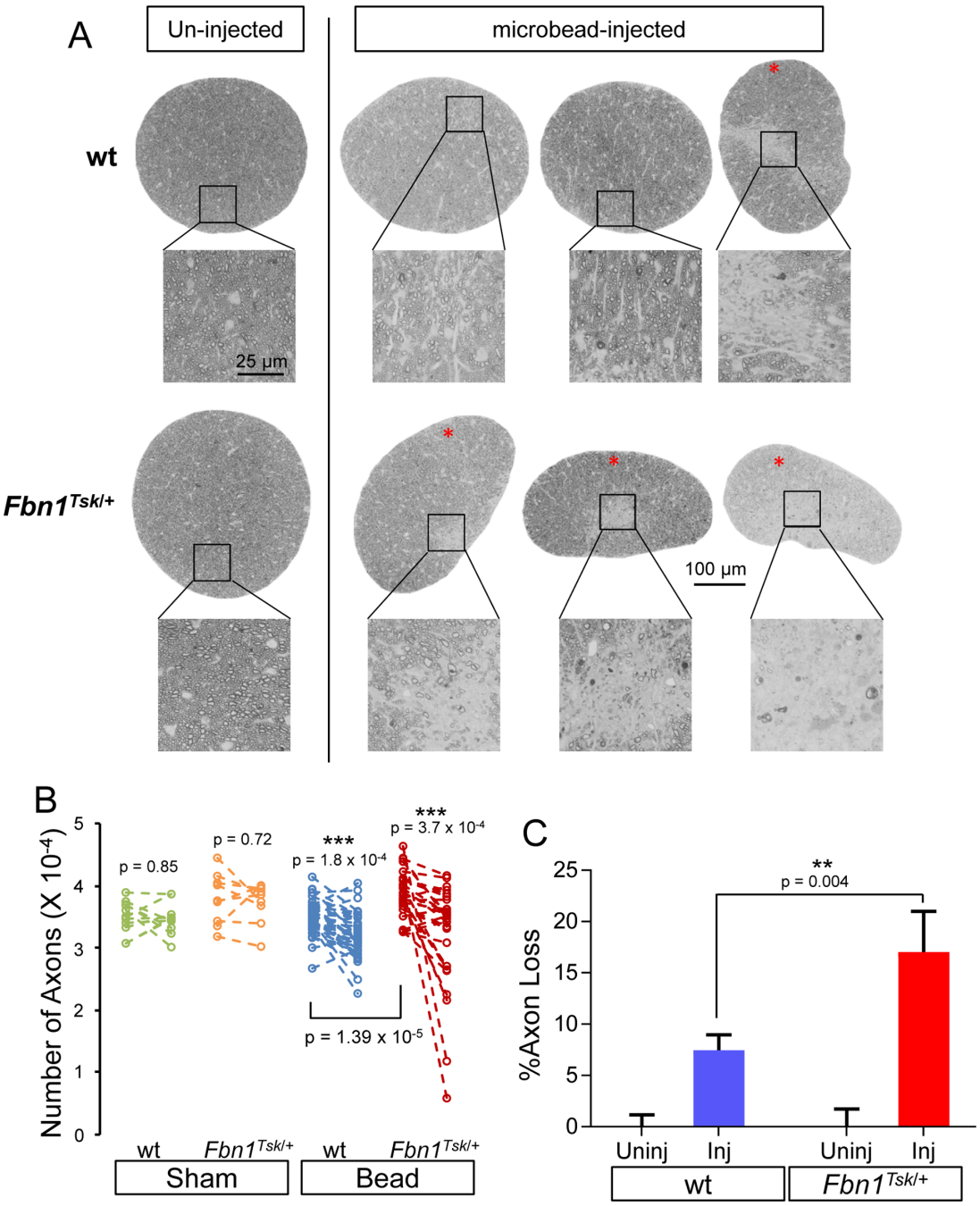

Figure 5. RGC Axon loss in response to microbead injection. Images of optic nerve cross-sections (**A**) show that compared to nerves from uninjected eyes (*left column*), microbead injection results in focal axon loss in some nerves (*red asterisks*), more commonly in *Fbn1*$^{Tsk/+}$ mice. Paired analysis (**B**) comparing uninjected (*left symbols*) with bead-injected eyes (*right symbols*) showed significant loss of axons for wt (*blue symbols*) and *Fbn1*$^{Tsk/+}$ mice (*red symbols*) but not for sham-injected controls (*green* and *orange symbols*). The average percent axon loss relative to the average number of axons in un-injected eyes (**C**) was lower for wt (*blue bar*) as compared to *Fbn1*$^{Tsk/+}$ mice (*red bar*). Numbers of microbead-injected animals: 43 wt and 29 *Fbn1*$^{Tsk/+}$: sham-injected: 12 wt and 9 *Fbn1*$^{Tsk/+}$. *Scale bar* for the whole nerve in A: 100 μm. *Dashed lines* connect paired nerves (**B**).

Discussion

Previously we reported several optic nerve phenotypes in *Fbn1*$^{Tsk/+}$ mice at normal IOP, including larger optic nerves, larger optic nerve axons and thinner pia mater at 6 and 16 months of age.[16] Although these differences did not result in fewer RGCs or RGC axons, we hypothesized that they could result in increased susceptibility to RGC degeneration if the *Fbn1*$^{Tsk/+}$ mice were challenged with elevated IOP. In the present study, we confirmed these alterations in optic nerve structure at normal IOP in *Fbn1*$^{Tsk/+}$ mice at 11 months of age (Figs. 2, 3, and 6). When IOP was elevated by injection of microbeads into the anterior chamber, loss of RGC cell bodies and axons was significantly greater in *Fbn1*$^{Tsk/+}$ mice

Investigative Ophthalmology & Visual Science

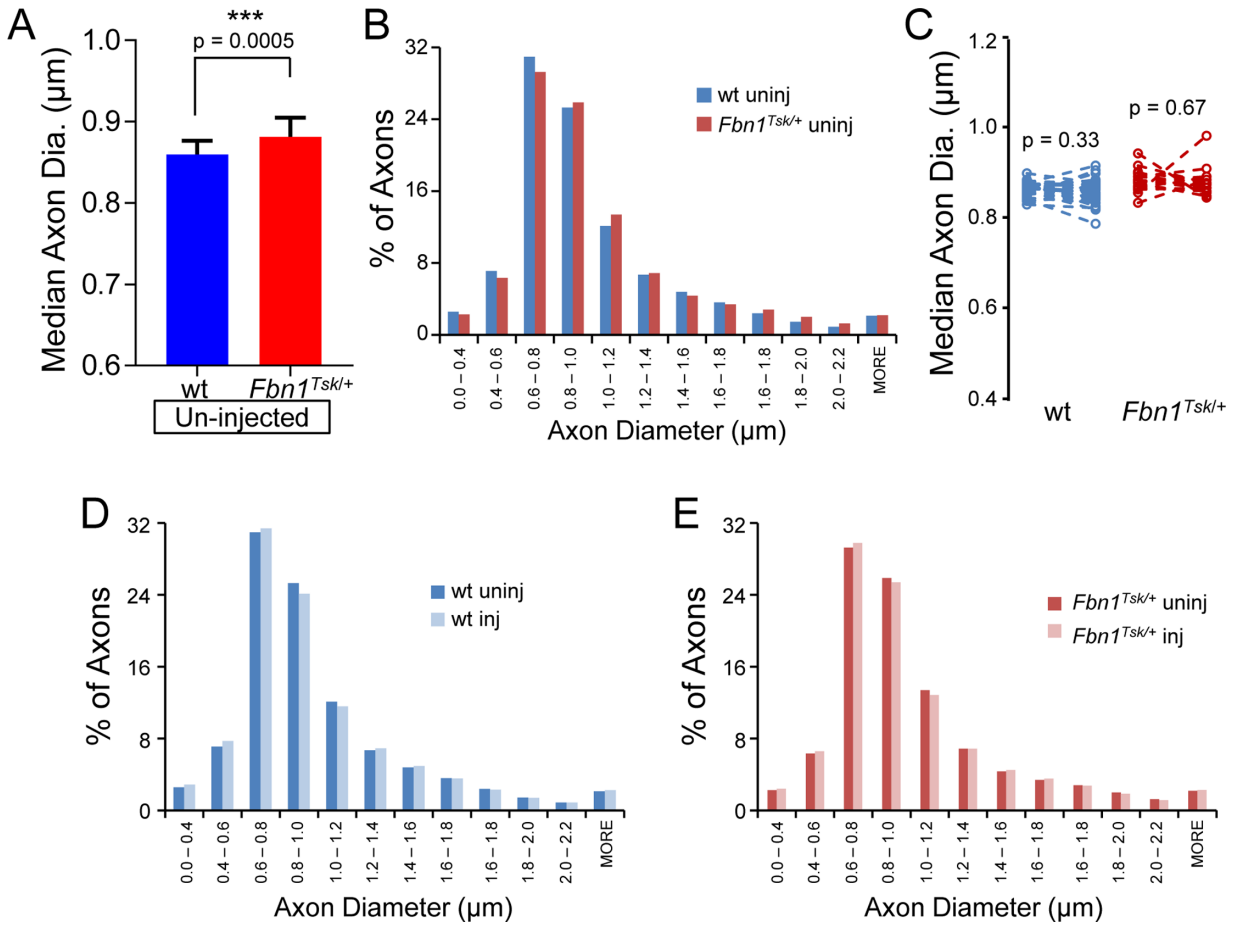

Figure 6. Optic nerve axon size. The median axon diameter of uninjected eyes (**A**) was larger in nerves from *Fbn1*$^{Tsk/+}$ mice (*red bar*) as compared with wt (*blue bar*). Histograms of pooled axon diameters of uninjected eyes (**B**) show a shift toward larger axons in *Fbn1*$^{Tsk/+}$ mice (*red bars*) compared with wt (*blue bars*). Paired analysis (**C**) comparing nerves from uninjected (*left symbols*) with those from bead-injected eyes (*right symbols*) showed no change in median axon diameter for wt (*blue symbols*) and *Fbn1*$^{Tsk/+}$ mice (*red symbols*). Histograms of pooled axon diameters were very similar for uninjected (*dark bars*) and microbead-injected (*light bars*) for wt (**D**) and *Fbn1*$^{Tsk/+}$ mice (**E**). Numbers of animals: 32 wt and 18 *Fbn1*$^{Tsk/+}$ (**A** and **C**). Numbers of axons included for each histogram: 1,105,075 for wt un-injected, 1,014,017 for wt injected, 684,888 for *Fbn1*$^{Tsk/+}$ un-injected and 616,953 for *Fbn1*$^{Tsk/+}$ injected (**B, D**, and **E**). *Dashed lines* connect paired eyes (**C**).

as compared with wt controls (Figs. 4 and 5), confirming our hypothesis of increased susceptibility to pressure-induced RGC degeneration.

There was considerable variation in susceptibility to microbead-induced RGC and optic nerve axon loss with relatively few mice showing very pronounced loss in the microbead-injected eye (Figs. 4B and 5B). This is not unexpected because axonopathy has been shown to be heterogeneous and asynchronous in multiple experimental models of glaucoma[44–48] and in the DBA/2J mouse model of inherited glaucoma.[49–52]

Although in general the amount of RGC death and axon loss varies considerably between studies and is dependent on specific methods of microbead injection, magnitude and duration of IOP elevation and age and strain of mice, the extent of loss in wt mice in our hands was on the lower side of other reported studies which more typically report approximately 10% to 30% axon loss with roughly similar IOP elevations.[37,38,53] However, Cone et al.[38] reported that older C57BL/6 mice are more resistant to IOP-induced damage compared with younger C57BL/6 mice. In that study, young mice two to four months of age had 7.5% loss of RGCs and 11.9% loss of optic axons, whereas older mice at 10 to 12 months of age had only 2.0% loss of RGCs and 5.2% loss of optic axons (tables 4 and 5 Cone et al.[38]). In the present study using the C57BL/6 strain, mice were of intermediate age of seven to 11 months and had losses intermediate to the young and old mice of Cone et al.[38] 5.8% RGC loss and 7.5% axon loss. Therefore, although somewhat low, the percentage loss of RGCs and axons is not inconsistent with previous studies.

The increased RGC degeneration occurred despite lower elevations of IOP in response to microbead injection, which resulted in an approximately 6 mmHg increase in wt mice (similar to IOP elevation in C57BL/6J mice reported by others[38,54,55]) compared with a 3-mm Hg increase in *Fbn1*$^{Tsk/+}$ mice (Fig. 1C). In our previous study, we found that *Fbn1*$^{Tsk/+}$ mice had thin corneas, which could lead to underestimation of IOP. However this was unlikely because we determined that tonometer calibrations were nearly identical in wt and *Fbn1*$^{Tsk/+}$ mice.[16] The *Tsk* mutation of *Fbn1* could affect IOP by disrupting elastic fibers. Within the trabecular meshwork, a dense network of elastic fibers is likely to contribute to the biomechanical properties of the

aqueous humor outflow pathway and thereby contribute to IOP regulation.[56,57] Fibrillin-1 microfibrils are essential for elastic fiber formation and contribute to their mechanical properties.[58] Elastic fiber structure is known to be affected by *Fbn1* mutations, including *Tsk*.[20,33] Although we did not directly investigate the mechanisms leading to reduced IOP responses, we did observe that clearance of microbeads tended to be more extensive and earlier in *Fbn1*$^{Tsk/+}$ mice (data not shown), which could have resulted in less efficient blockage of the iridocorneal angle.

IOP appeared to steadily decrease in bead-injected and uninjected eyes of *Fbn1*$^{Tsk/+}$ mice starting at about 30 days after injection (Fig. 1B). Although we saw age-dependent declines in IOP in our previous work,[16] in the present study the decline was more rapid and due to lower values. Although in the previous study, IOP was measured every three months,[16] in the present study, IOP was measured repeatedly, every three to six days. It is possible that repeated measurements of IOP under anesthesia resulted in reduced IOP of *Fbn1*$^{Tsk/+}$ mice.

In this study, the contralateral uninjected eyes served as intra-animal controls for the bead-injected eyes. The contralateral eye likely does respond to elevation of IOP in the bead-injected eye, because previous studies have shown changes such as activation of retinal microglial cells in the contralateral control eyes of mice with unilaterally elevated IOP.[59,60] Contralateral responses have been shown to not include loss of RGC axons in wt 129S6 mice.[61] However, in mice carrying a deletion in the *INK4* locus, loss of RGCs in the retinas of contralateral eyes has been reported.[61] In our study, we included an additional control of sham-injected mice for which microbeads were omitted from the anterior chamber injection while the contralateral eye was left uninjected. For sham-injected wt or *Fbn1*$^{Tsk/+}$ mice, anterior chamber injection did not result in elevated IOP. Comparing un-injected eyes from sham-injected and microbead-injected groups, RGC and axon numbers were similar, indicating that there was no significant loss in eyes contralateral to microbead-injected eyes. Therefore our uninjected contralateral and sham-injected controls support loss of RGCs and optic nerve axons specifically as a result of microbead injection, which resulted in elevated IOP.

We confirmed that the optic nerves of *Fbn1*$^{Tsk/+}$ mice are significantly larger in cross-sectional area as compared with wt and that the enlargement of the optic nerve coincides with thinning of the pia mater, as we reported previously.[16] These findings suggest altered biomechanical properties of the optic nerve, consistent with known differences associated with the *Tsk* mutation of fibrillin-1 in the biomechanics of other tissues, such as the skin and lung.[62,63] At a molecular level in *Fbn1*$^{Tsk/+}$ mice, alterations of biomechanics and tissue structure originate from the copolymerization of the *Tsk* and normal forms of the fibrillin-1 protein, which results in the formation of abnormal microfibrils.[33,64] Microfibrils are required for proper formation of elastic fibers,[58] which likely make significant contributions to the mechanical properties of the pia mater, thereby contributing to the biomechanical responses of the optic nerve to pressure changes.[65,66] In addition, microfibrils regulate growth factors such as transforming growth factor β that in turn regulate production of other extracellular matrix proteins, a process that is known to be perturbed by mutations in *Fbn1*.[13,67] Alterations in the biomechanics of the optic nerve have long been postulated to contribute to glaucoma pathogenesis.[68] We speculate that thinning of the pia mater may allow for expansion due to interstitial tissue pressure within the optic nerve.[14] Microbead injection resulted in reduction of nerve size and thickening of the pia mater, suggesting tissue remodeling in response to elevated IOP.

Expansion of the optic nerve appears to be associated with aging, which is a significant risk factor for glaucoma, as we previously reported with C57BL/6 mice[16] and others have reported for DBA/2J mice and rats.[34,69] Smith et al.[70] found that before extensive axon loss, the optic nerves of the glaucoma model DBA/2J mice were significantly enlarged compared with the appropriate D2G controls, suggesting that acceleration of optic nerve expansion, as we have found for *Fbn1*$^{Tsk/+}$ mice, may also be a component of the pathogenesis of glaucoma. In response to microbead injection, optic nerve size was reduced 4.2% for wt and 11.1% for *Fbn1*$^{Tsk/+}$ mice as compared with uninjected controls. Percent nerve reduction was significantly correlated with percent axon loss ($R^2 = 0.45$, $P < 0.001$), suggesting that reduction of nerve size resulted from loss of axons.

We also confirmed in this study that the distribution of axon sizes was shifted to larger diameters in the optic nerves of *Fbn1*$^{Tsk/+}$ mice (Figs. 6 A, 6B). Axon size is precisely regulated in central nervous system nerve tracts to optimize efficiency of information transfer and to minimize energy costs within spatial constraints.[71,72] Small axons tend to predominate because of efficiency of information transfer, whereas larger axons allow for faster propagation of action potentials and more rapid firing rates and are capable of driving larger numbers of active zones.[71] The distribution of axon sizes in the optic nerve is remarkably similar across species, with a strong skew toward smaller sizes,[72] as found in this study. Axon size is determined by several factors, including axonal membrane-associated microtubule organizing complexes and actin and neurofilament cytoskeletal elements.[73–75] Cytoskeletal elements, including those of RGC axons, are regulated by interactions with the extracellular matrix.[76] Fibrillin-1 expressed in the optic nerve could interact with axons and alter the cytoskeleton, perhaps through its arginine-glycine-aspartic acid (RGD) domain interacting with integrins, or by changing the biomechanical properties of the extracellular matrix.[77] Although we do not know the mechanism, our data show that the fundamental parameter of axon caliber is dysregulated as a result of the *Tsk* mutation of *Fbn1* and suggest a critical and previously unknown role for fibrillin-1 in determining axon size in the optic nerve.

Axon enlargement in this study with 11-month-old C57BL/6J mice (Figs. 6A, 6B) is consistent with our previous work showing age-dependent axon expansion in the optic nerves of six- and 16-month-old C57BL/6J mice.[16] Optic nerve axon size has also been shown to be enlarged in DBA/2J mice, with age-dependent expansion.[70] Age-dependent axon enlargement has also been shown in the human optic nerve.[78,79] These findings in mice and humans suggest that axon enlargement in the optic nerve may be a normal component of aging and could be a factor in neurodegenerative diseases, such as glaucoma, for which age is an important risk factor. Consistent with this, Stahon et al.[35] showed that age-dependent enlargement of optic nerve axons coincided with altered mitochondrial morphology and lowered axonal ATP levels, suggesting compromised metabolic capacity in axons enlarged through aging.

Studies from the 1980s and 1990s by Quigley et al.[80,81] and Repka and Quigly[82] extensively considered the signif-

Investigative Ophthalmology & Visual Science

icance of axon caliber in susceptibility to glaucomatous degeneration. In a monkey model of elevated IOP, a shift in the distribution of remaining axons towards smaller diameters could be seen in nerves with modest damage, and analysis of loss at each size category indicated greater loss for larger axons.[81,83] Similarly, in optic nerves from glaucoma patients, the distributions of remaining axons was shifted toward smaller sizes compared with normal nerves, the magnitude of which correlated with the extent of damage, suggesting preferential loss of large diameter axons.[80] However, smaller-diameter axons have also been suggested to be more vulnerable to pressure-induced damage. Measuring compound action potentials of isolated mouse optic nerves, Baltan et al.[84] showed loss of signal from slow-conducting axons and reduced numbers of small- and medium-sized axons in response to elevated IOP in the DBA/2J mouse model, which they attributed to reduced metabolic capacity.

We had hypothesized that enlarged axons would be more vulnerable to pressure-induced RGC degeneration. Confirming our hypothesis, *Fbn1*$^{Tsk/+}$ mice with their enlarged axons did have greater pressure-induced loss of RGCs and optic nerve axons than did wt (Figs. 4 and 5). Comparisons of median axon diameter of individual mice did not show significant changes in axon size (Fig. 6C). However, analysis of pooled axons from all mice in each group showed a slight (<1%) reduction in median axon diameter on microbead injection, suggesting a very slight preference for loss of larger than average size axons. On the other hand, the axon size distributions are very similar for bead injected and uninjected nerves (Figs. 6D, 6E) with little or no reduction in percentage of larger category axons, 1.2 μm in diameter and above, arguing against selective susceptibility of large axons. Analysis of size distribution including only mice with >20% axon loss or only those with 5% to 20% loss yielded similar results. Our results suggest the possibility that enlargement above normal size, as occurs through aging, rather than above a certain size threshold, renders RGCs and their axons more vulnerable to pressure-induced damage.

There was considerably more variability in phenotypes of *Fbn1*$^{Tsk/+}$ mice as compared with wt (Figs. 2B, 3C, 4B, 5B). A previous study showed similar intraindividual variability arising from another mutation in *Fbn1* in a genetically homogeneous mouse line.[85] Intraindividual differences in phenotypes caused by genetic mutations are known to occur even in mice with identical genetic backgrounds because of epigenetic modifications,[86] which could be a possible explanation for the higher variability of *Fbn1*$^{Tsk/+}$ mice found in this study.

Comparing uninjected eyes, the number of axons and RGCs were significantly higher for *Fbn1*$^{Tsk/+}$ compared with wt mice at 11 months of age (Figs. 4B, 5B). In a previous study by Wu et al.,[16] we found that the number of axons and RGCs was not significantly different between wt and *Fbn1*$^{Tsk/+}$ mice at 16 months of age. This discrepancy might be due to age differences but more likely is methodological because in Wu et al.,[16] we manually counted axons and RGCs, whereas for the present study we used automated counting programs.

In summary, we have shown that *Fbn1*$^{Tsk/+}$ mice had greater loss of RGC cell bodies in the retina and RGC axons in the optic nerve, despite having lower IOP responses. We also found that the *Tsk* mutation of *Fbn1* results in enlargement of optic nerve axons, suggesting a previously unknown role for fibrillin-1 in determining axon caliber. The greater vulnerability of *Fbn1*$^{Tsk/+}$ mice to pressure-induced RGC degeneration may be due to accelerated age-dependent axon enlargement which may result in decreased metabolic capacity and reduced capability to withstand mechanical stresses resulting from elevated IOP. Further study will investigate the mechanisms by which fibrillin-1 contributes to axon enlargement and the functional implications of enlarged optic nerve and optic nerve axons.

Acknowledgments

Supported by NIH Grant R01EY020894 (RWK) and Vanderbilt Vision Research Center (P30EY008126); Departmental Unrestricted Award from Research to Prevent Blindness, Inc.; Vanderbilt Cell Imaging Shared Resource.

Disclosure: **H.-J. Wu,** None; **J. Kuchtey,** None; **R.W. Kuchtey,** None

References

1. Calkins DJ. Critical pathogenic events underlying progression of neurodegeneration in glaucoma. *Prog Retin Eye Res*. 2012;31:702–719.
2. Quigley HA. Neuronal death in glaucoma. *Prog Retin Eye Res*. 1999;18:39–57.
3. Burgoyne CF, Crawford Downs J, Bellezza AJ, Francis Suh J-K, Hart RT. The optic nerve head as a biomechanical structure: a new paradigm for understanding the role of IOP-related stress and strain in the pathophysiology of glaucomatous optic nerve head damage. *Prog Retin Eye Res*. 2005;24:39–73.
4. Bellezza AJ, Rintalan CJ, Thompson HW, Downs JC, Hart RT, Burgoyne CF. Deformation of the Lamina Cribrosa and Anterior Scleral Canal Wall in Early Experimental Glaucoma. *Invest Ophthalmol Vis Sci*. 2003;44:623–637.
5. Yan DB, Coloma FM, Metheetrairut A, Trope GE, Heathcote JG, Ethier CR. Deformation of the lamina cribrosa by elevated intraocular pressure. *Br J Ophthalmol*. 1994;78:643–648.
6. Yang H, Downs JC, Girkin C, et al. 3-D histomorphometry of the normal and early glaucomatous monkey optic nerve head: lamina cribrosa and peripapillary scleral position and thickness. *Invest Ophthalmol Vis Sci*. 2007;48:4597–4607.
7. Sigal IA, Flanagan JG, Tertinegg I, Ethier CR. Finite element modeling of optic nerve head biomechanics. *Invest Ophthalmol Vis Sci*. 2004;45:4378–4387.
8. Sigal IA, Bilonick RA, Kagemann L, et al. The optic nerve head as a robust biomechanical system. *Invest Ophthalmol Vis Sci*. 2012;53:2658–2667.
9. Eilaghi A, Flanagan JG, Simmons CA, Ethier CR. Effects of scleral stiffness properties on optic nerve head biomechanics. *Ann Biomed Eng*. 2010;38:1586–1592.
10. Bellezza AJ, Hart RT, Burgoyne CF. The optic nerve head as a biomechanical structure: initial finite element modeling. *Invest Ophthalmol Vis Sci*. 2000;41:2991–3000.
11. Sigal IA, Flanagan JG, Tertinegg I, Ethier CR. Predicted extension, compression and shearing of optic nerve head tissues. *Exp Eye Res*. 2007;85:312–322.
12. Sigal IA, Ethier CR. Biomechanics of the optic nerve head. *Exp Eye Res*. 2009;88:799–807.
13. Ramirez F, Sakai LY. Biogenesis and function of fibrillin assemblies. *Cell Tissue Res*. 2010;339:71.
14. Morgan WH, Yu DY, Alder VA, et al. The correlation between cerebrospinal fluid pressure and retrolaminar tissue pressure. *Invest Ophthalmol Vis Sci*. 1998;39:1419–1428.
15. Balaratnasingam C, Morgan WH, Johnstone V, Pandav SS, Cringle SJ, Yu D-Y. Histomorphometric measurements in

human and dog optic nerve and an estimation of optic nerve pressure gradients in human. *Exp Eye Res*. 2009;89: 618–628.
16. Wu H-J, Hazlewood RJ, Kuchtey J, Kuchtey RW. Enlarged optic nerve axons and reduced visual function in mice with defective microfibrils. *eNeuro*. 2018;5.
17. Humphrey JD, Schwartz MA, Tellides G, Milewicz DM. Role of mechanotransduction in vascular biology: focus on thoracic aortic aneurysms and dissections. *Circ Res*. 2015;116:1448–1461.
18. Humphrey JD, Milewicz DM, Tellides G, Schwartz MA. Dysfunctional mechanosensing in aneurysms. *Science*. 2014;344:477–479.
19. Judge DP, Biery NJ, Keene DR, et al. Evidence for a critical contribution of haploinsufficiency in the complex pathogenesis of Marfan syndrome. *J Clin Invest*. 2004;114: 172–181.
20. Habashi JP, Judge DP, Holm TM, et al. Losartan, an AT1 antagonist, prevents aortic aneurysm in a mouse model of Marfan syndrome. *Science*. 2006;312:117–121.
21. Izquierdo NJ, Traboulsi EI, Enger C, Maumenee IH. Glaucoma in the Marfan syndrome. *Trans Am Ophthalmol Soc*. 1992;90:111–122.
22. Park H-YL, Kim JH, Jung Y, Park CK. Racial differences in the extracellular matrix and histone acetylation of the lamina cribrosa and peripapillary sclera. *Invest Ophthalmol Vis Sci*. 2017;58:4143–4154.
23. Schlötzer-Schrehardt U, Hammer CM, Krysta AW, et al. LOXL1 deficiency in the lamina cribrosa as candidate susceptibility factor for a pseudoexfoliation-specific risk of glaucoma. *Ophthalmology*. 2012;119:1832–1843.
24. Zenkel M, Schlötzer-Schrehardt U. Expression and regulation of LOXL1 and elastin-related genes in eyes with exfoliation syndrome. *J Glaucoma*. 2014;23:S48
25. Kuchtey J, Kunkel J, Esson D, et al. Screening *ADAMTS10* in dog populations supports Gly661Arg as the glaucoma-causing variant in beagles. *Invest Opthalm Vis Sci*. 2013;54:1881.
26. Ahonen SJ, Kaukonen M, Nussdorfer FD, Harman CD, Komáromy AM, Lohi H. A novel missense mutation in ADAMTS10 in Norwegian elkhound primary glaucoma. *PLOS ONE*. 2014;9:e111941.
27. Forman OP, Pettitt L, Komáromy AM, Bedford P, Mellersh C. A novel genome-wide association study approach using genotyping by exome sequencing leads to the identification of a primary open angle glaucoma associated inversion disrupting ADAMTS17. *PLOS ONE*. 2015;10:e0143546.
28. Oliver JAC, Forman OP, Pettitt L, Mellersh CS. Two independent mutations in ADAMTS17 are associated with primary open angle glaucoma in the basset hound and basset Fauve de Bretagne breeds of dog. *PLOS ONE*. 2015;10:e0140436.
29. Springelkamp H, Höhn R, Mishra A, et al. Meta-analysis of genome-wide association studies identifies novel loci that influence cupping and the glaucomatous process. *Nat Comm*. 2014;5:4883.
30. Springelkamp H, Mishra A, Hysi PG, et al. Meta-analysis of genome-wide association studies identifies novel loci associated with optic disc morphology. *Genet Epidemiol*. 2015;39:207–216.
31. Springelkamp H, Iglesias AI, Mishra A, et al. New insights into the genetics of primary open-angle glaucoma based on meta-analyses of intraocular pressure and optic disc characteristics. *Hum Mol Genet*. 2017;26:438–453.
32. Kuchtey J, Kuchtey RW. The microfibril hypothesis of glaucoma: implications for treatment of elevated intraocular pressure. *J Ocular Pharmacol Therap*. 2014;30:170–180.
33. Kielty CM, Raghunath M, Siracusa LD, et al. The tight skin mouse: demonstration of mutant fibrillin-1 production and assembly into abnormal microfibrils. *J Cell Biol*. 1998;140:1159–1166.
34. Cooper ML, Crish SD, Inman DM, Horner PJ, Calkins DJ. Early astrocyte redistribution in the optic nerve precedes axonopathy in the DBA/2J mouse model of glaucoma. *Exp Eye Res*. 2016;150:22−33.
35. Stahon KE, Bastian C, Griffith S, Kidd GJ, Brunet S, Baltan S. Age-related changes in axonal and mitochondrial ultrastructure and function in white matter. *J Neurosci*. 2016;36:9990–10001.
36. Zhu Y, Pappas AC, Wang R, Seifert P, Sun D, Jakobs TC. Ultrastructural morphology of the optic nerve head in aged and glaucomatous mice. *Invest Ophthalmol Vis Sci*. 2018;59:3984–3996.
37. Steinhart MR, Cone-Kimball E, Nguyen C, et al. Susceptibility to glaucoma damage related to age and connective tissue mutations in mice. *Exp Eye Res*. 2014;119:54–60.
38. Cone FE, Gelman SE, Son JL, Pease ME, Quigley HA. Differential susceptibility to experimental glaucoma among 3 mouse strains using bead and viscoelastic injection. *Exp Eye Res*. 2010;91:415–424.
39. Ding C, Wang P, Tian N. Effect of general anesthetics on IOP in elevated IOP mouse model. *Exp Eye Res*. 2011;92:512–520.
40. Aihara M, Lindsey JD, Weinreb RN. Twenty-four-hour pattern of mouse intraocular pressure. *Exp Eye Res*. 2003;77:681–686.
41. Nadal-Nicolás FM, Jiménez-López M, Salinas-Navarro M, et al. Whole number, distribution and co-expression of Brn3 transcription factors in retinal ganglion cells of adult albino and pigmented rats. *PLoS One*. 2012;7:e49830.
42. Geeraerts E, Dekeyster E, Gaublomme D, Salinas-Navarro M, De Groef L, Moons L. A freely available semi-automated method for quantifying retinal ganglion cells in entire retinal flatmounts. *Exp Eye Res*. 2016;147:105–113.
43. Zarei K, Scheetz TE, Christopher M, et al. Automated axon counting in rodent optic nerve sections with AxonJ. *Sci Rep*. 2016;6:26559.
44. Calkins DJ. Critical pathogenic events underlying progression of neurodegeneration in glaucoma. *Prog Retin Eye Res*. 2012;31:702–719.
45. Nickells RW, Howell GR, Soto I, John SWM. Under pressure: cellular and molecular responses during glaucoma, a common neurodegeneration with axonopathy. *Ann Rev Neurosci*. 2012;35:153–179.
46. Vidal-Sanz M, Salinas-Navarro M, Nadal-Nicolás FM, et al. Understanding glaucomatous damage: anatomical and functional data from ocular hypertensive rodent retinas. *Prog Retin Eye Res*. 2012;31:1–27.
47. Salinas-Navarro M, Alarcón-Martínez L, Valiente-Soriano FJ, et al. Ocular hypertension impairs optic nerve axonal transport leading to progressive retinal ganglion cell degeneration. *Exp Eye Res*. 2010;90:168–183.
48. Soto I, Pease ME, Son JL, Shi X, Quigley HA, Marsh-Armstrong N. Retinal ganglion cell loss in a rat ocular hypertension model is sectorial and involves early optic nerve axon loss. *Invest Ophthalmol Vis Sci*. 2011;52:434–441.
49. Bosco A, Crish SD, Steele MR, et al. early reduction of microglia activation by irradiation in a model of chronic glaucoma. *PLoS One*. 2012;7.
50. Howell GR, Libby RT, Jakobs TC, et al. Axons of retinal ganglion cells are insulted in the optic nerve early in DBA/2J glaucoma. *J Cell Biol*. 2007;179:1523–1537.
51. John SWM, Smith RS, Savinova OV, et al. Essential iris atrophy, pigment dispersion, and glaucoma in DBA/2J mice. *Invest Ophthalmol Vis Sci*. 1998;39:951–962.

Investigative Ophthalmology & Visual Science

52. Schuettauf F, Rejdak R, Walski M, et al. Retinal neurodegeneration in the DBA/2J mouse—a model for ocular hypertension. *Acta Neuropathol*. 2004;107:352–358.
53. Morgan JE, Tribble JR. Microbead models in glaucoma. *Exp Eye Res*. 2015;141:9–14.
54. Sappington RM, Carlson BJ, Crish SD, Calkins DJ. The microbead occlusion model: a paradigm for induced ocular hypertension in rats and mice. *Invest Ophthalmol Vis Sci*. 2010;51:207–216.
55. Frankfort BJ, Khan AK, Tse DY, et al. Elevated intraocular pressure causes inner retinal dysfunction before cell loss in a mouse model of experimental glaucoma. *Invest Ophthalmol Vis Sci*. 2013;54:762–770.
56. Overby DR, Bertrand J, Schicht M, Paulsen F, Stamer WD, Lütjen-Drecoll E. The structure of the trabecular meshwork, its connections to the ciliary muscle, and the effect of pilocarpine on outflow facility in mice. *Invest Ophthalmol Vis Sci*. 2014;55:3727–3736.
57. Hann CR, Fautsch MP. The elastin fiber system between and adjacent to collector channels in the human juxtacanalicular tissue. *Invest Ophthalmol Vis Sci*. 2011;52:45–50.
58. Baldwin AK, Simpson A, Steer R, Cain SA, Kielty CM. Elastic fibres in health and disease. *Exp Rev Mol Med*. 2013;15:e8.
59. Ramírez AI, de Hoz R, Fernández-Albarral JA, et al. Time course of bilateral microglial activation in a mouse model of laser-induced glaucoma. *Sci Rep*. 2020;10:4890.
60. Gallego BI, Salazar JJ, de Hoz R, et al. IOP induces upregulation of GFAP and MHC-II and microglia reactivity in mice retina contralateral to experimental glaucoma. *J Neuroinflammation*. 2012;9:92.
61. Gao S, Jakobs TC. Mice homozygous for a deletion in the glaucoma susceptibility locus ink4 show increased vulnerability of retinal ganglion cells to elevated intraocular pressure. *Am J Pathol*. 2016;186:985–1005.
62. Menton DN, Hess RA, Lichtenstein JR, Eisen AZ. The structure and tensile properties of the skin of tight-skin (Tsk) mutant mice. *J Invest Dermatol*. 1978;70:4–10.
63. Ito S, Bartolák-Suki E, Shipley JM, Parameswaran H, Majumdar A, Suki B. Early emphysema in the tight skin and pallid mice: roles of microfibril-associated glycoproteins, collagen, and mechanical forces. *Am J Respir Cell Mol Biol*. 2006;34:688–694.
64. Gayraud B, Keene DR, Sakai LY, Ramirez F. New insights into the assembly of extracellular microfibrils from the analysis of the fibrillin 1 mutation in the tight skin mouse. *J Cell Biol*. 2000;150:667–680.
65. Feola AJ, Myers JG, Raykin J, et al. Finite element modeling of factors influencing optic nerve head deformation due to intracranial pressure. *Invest Ophthalmol Vis Sci*. 2016;57:1901–1911.
66. Hua Y, Tong J, Ghate D, Kedar S, Gu L. Intracranial pressure influences the behavior of the optic nerve head. *J Biomech Eng*. 2017;139:031003-031003-031006.
67. Ramirez F, Rifkin DB. Extracellular microfibrils: contextual platforms for TGFβ and BMP signaling. *Curr Opin Cell Biol*. 2009;21:616–622.
68. Stowell C, Burgoyne CF, Tamm ER, et al. Biomechanical aspects of axonal damage in glaucoma: a brief review. *Exp Eye Res*. 2017;157:13–19.
69. Cavallotti C, Cavallotti D, Pescosolido N, Pacella E. Age-related changes in rat optic nerve: morphological studies. *Anat Histol Embryol*. 2003;32:12–16.
70. Smith MA, Plyler ES, Dengler-Crish CM, Meier J, Crish SD. Nodes of Ranvier in glaucoma. *Neuroscience*. 2018;390:104–118.
71. Perge JA, Niven JE, Mugnaini E, Balasubramanian V, Sterling P. Why do axons differ in caliber? *J Neurosci*. 2012;32:626–638
72. Perge JA, Koch K, Miller R, Sterling P, Balasubramanian V. How the Optic Nerve Allocates Space, Energy Capacity, and Information. *J Neurosci*. 2009;29:7917–7928.
73. Stephan R, Goellner B, Moreno E, et al. Hierarchical microtubule organization controls axon caliber and transport and determines synaptic structure and stability. *Dev Cell*. 2015;33:5–21.
74. Leite SC, Sampaio P, Sousa VF, et al. The actin-binding protein α-adducin is required for maintaining axon diameter. *Cell Rep*. 2016;15:490–498.
75. Fan A, Tofangchi A, Kandel M, Popescu G, Saif T. Coupled circumferential and axial tension driven by actin and myosin influences in vivo axon diameter. *Sci Rep*. 2017;7:1–12.
76. Vecino E, Heller JP, Veiga-Crespo P, Martin KR, Fawcett JW. Influence of extracellular matrix components on the expression of integrins and regeneration of adult retinal ganglion cells. *PLoS One*. 2015;10:e0125250.
77. Zeyer KA, Reinhardt DP. Fibrillin-containing microfibrils are key signal relay stations for cell function. *J Cell Commun Signal*. 2015;9:309–325.
78. Jonas JB, Schmidt AM, Müller-Bergh JA, Schlötzer-Schrehardt UM, Naumann GO. Human optic nerve fiber count and optic disc size. *Invest Ophthalmol Vis Sci*. 1992;33:2012–2018.
79. Mikelberg FS, Yidegiligne HM, White VA, Schulzer M. Relation between optic nerve axon number and axon diameter to scleral canal area. *Ophthalmology*. 1991;98:60–63.
80. Quigley HA, Dunkelberger GR, Green WR. Chronic Human Glaucoma Causing Selectively Greater Loss of Large Optic Nerve Fibers. *Ophthalmology*. 1988;95:357–363.
81. Quigley HA, Sanchez RM, Dunkelberger GR, L'Hernault NL, Baginski TA. Chronic glaucoma selectively damages large optic nerve fibers. *Invest Ophthalmol Vis Sci*. 1987;28:913–920.
82. Repka MX, Quigley HA. The effect of age on normal human optic nerve fiber number and diameter. *Ophthalmology*. 1989;96:26–32.
83. Glovinsky Y, Quigley HA, Dunkelberger GR. Retinal ganglion cell loss is size dependent in experimental glaucoma. *Invest Ophthalmol Vis Sci*. 1991;32:484–491.
84. Baltan S, Inman DM, Danilov CA, Morrison RS, Calkins DJ, Horner PJ. Metabolic vulnerability disposes retinal ganglion cell axons to dysfunction in a model of glaucomatous degeneration. *J Neurosci*. 2010;30:5644–5652.
85. Lima BL, Santos EJC, Fernandes GR, et al. A new mouse model for Marfan syndrome presents phenotypic variability associated with the genetic background and overall levels of Fbn1 expression. *PLoS One*. 2010;5:e14136.
86. Bertozzi TM, Ferguson-Smith AC. Metastable epialleles and their contribution to epigenetic inheritance in mammals. *Semin Cell Dev Biol*. 2020;97:93–105.

Investigative Ophthalmology & Visual Science